BABINET'S PRINCIPLE IN ACOUSTICS: A TIME-DOMAIN REAPPRAISAL

C Feuillade Institute of Physics, Pontificia Universidad Católica de Chile, Avenida Vicuña Mackenna 4860, Santiago, Chile

1. INTRODUCTION

A representative account of Babinet's principle applied to optics is given by Brooker[1]. If light waves are considered spatial variations of a scalar function, and a Kirchhoff boundary condition and the Kirchhoff integral[2] applied, the sum of two wave fields received at a point downstream from two complementary apertures, whose opaque and transparent areas are interchanged, where the reception point is in the same relation to both apertures, is the same as the wave field from the unobstructed wave front. Let the field amplitude at point **r** in the forward propagation direction from an aperture *A* be $U_A(\mathbf{r})$, and the amplitude for the second complementary aperture *B* be $U_B(\mathbf{r})$. In the direct geometrical line of propagation from the source, these two components add to give the same field that would be observed if neither aperture were present. Away from this line, if no unobstructed propagation from the source is received, any field detected when the apertures are present must be due to diffraction at the aperture edges. However, since no diffractions would occur if no aperture were present, the diffracted field amplitudes from the two apertures must cancel each other, i.e., $U_A(\mathbf{r}) = - U_B(\mathbf{r})$. This also implies that $|U_A(\mathbf{r})|^2 = |U_B(\mathbf{r})|^2$, so that the diffracted *intensities* from the two complementary apertures should be identical. This description thereby reveals two separate statements that summarize Babinet's principle: (a) the aggregate field from two complementary apertures is the same as if neither aperture were present; (b) the diffracted fields from the two apertures cancel in amplitude, but have the same intensity distribution.

Here, a time-domain description of Babinet's principle is given for the acoustic case. The Biot and Tolstoy (BT) closed form, normal coordinate, theory for the acoustic pressure impulse response of a rigid wedge[3-5], together with a later extension to pressure-release wedges by Kinney *et al*.[6], are used to investigate Babinet's principle in acoustics for screens consisting of pairs of horizontally-opposed semi-infinite half-planes. BT provides *exact* analytical expressions for the impulse response from point-source to point-receiver, and avoids the Kirchhoff approximation. It also shows that the impulse response has two causally related, but independently propagating, time-separated components: (a) direct arrivals from the source itself, or from images of the source reflected in the faces of the half-plane or wedge; (b) diffraction arrivals from the apex of the half-plane or wedge. The diffractions always arrive *after* the direct/reflected signals have passed. By reformulating the interaction of the incident field with a screen in the time-domain, these two phenomena become mathematically separable, and emerge as the clear physical antecedents for the two statements of Babinet's principle summarized above. This approach demonstrates that the statement that the aggregate field from two complementary screens is the same as if neither were present applies to the *direct* arrivals, irrespective of the boundary conditions. It also shows how the amplitudes of the *diffracted* arrivals, generated by complementary screens with opposite boundary conditions, cancel each other in the forward scattering direction, but have the same intensity.

2. BIOT-TOLSTOY THEORY

2.1. The BT field equations

BT uses cylindrical coordinates to represent the acoustic field, as shown in Figure 1. The source is placed at (r_o, θ_o, z_o), and the receiver at (r_r, θ_r, z_r), and the wedge angle is $0 < \theta_w \leq 2\pi$. For a rigid wedge, with reflectivity $R = +1$ at the wedge surfaces, the impulse pressure amplitude is given by[3]

$$p_{rig}(r_r, \theta_r, z_r, t) = \frac{2S\rho c^2}{\pi \theta_w} \sum_n \cos \nu_n \theta_o \cos \nu_n \theta_r \, I_n \ , \qquad (1)$$

and for a pressure-release wedge $R = -1$ at the surfaces, and the impulse response amplitude is[6]

$$p_{p\text{-}r}(r_r, \theta_r, z_r, t) = \frac{2S\rho c^2}{\pi\theta_w} \sum_n \sin \nu_n\theta_o \sin \nu_n\theta_r \, I_n \,, \tag{2}$$

where:

$$\begin{aligned} I_n &= 0 && (t < t_0)\,; \\ &= (1/2c r_o r_r \sin\xi)\, \cos \nu_n\xi && (t_0 \le t \le \tau_0)\,; \\ &= (-1/2c r_o r_r \sinh\eta)\, \sin \nu_n\pi e^{-\nu_n\eta} && (t \ge \tau_0), \end{aligned} \tag{3}$$

and:

$$\begin{aligned} \xi &= \cos^{-1}\left[(r_o^2 + r_r^2 + z^2 - c^2t^2)/2r_o r_r\right] \quad (|\,\xi\,| \le \pi)\ ; \\ \eta &= \cosh^{-1}\left[\left(c^2t^2 - (r_o^2 + r_r^2 + z^2)\right)/2r_o r_r\right]\ ; \\ t_0 &= (1/c)\left[(r_o - r_r)^2 + z^2\right]^{1/2}\ ; \\ \tau_0 &= (1/c)\left[(r_o + r_r)^2 + z^2\right]^{1/2}\ , \end{aligned} \tag{4}$$

The parameter $z = (z_r - z_o)$ is the axial distance along the apex from source to receiver. The time t_0 is the earliest arrival time for a *direct* source-receiver transmission for given r_o, r_r, and z, and τ_0 is the earliest arrival time for a transmission passing from the source to the apex, and then to the receiver. S represents the "strength" of the acoustic pressure source, and ρ is the density of the propagation medium. The parameter $\nu_n = n\nu$, where $\nu = \pi/\theta_w$.

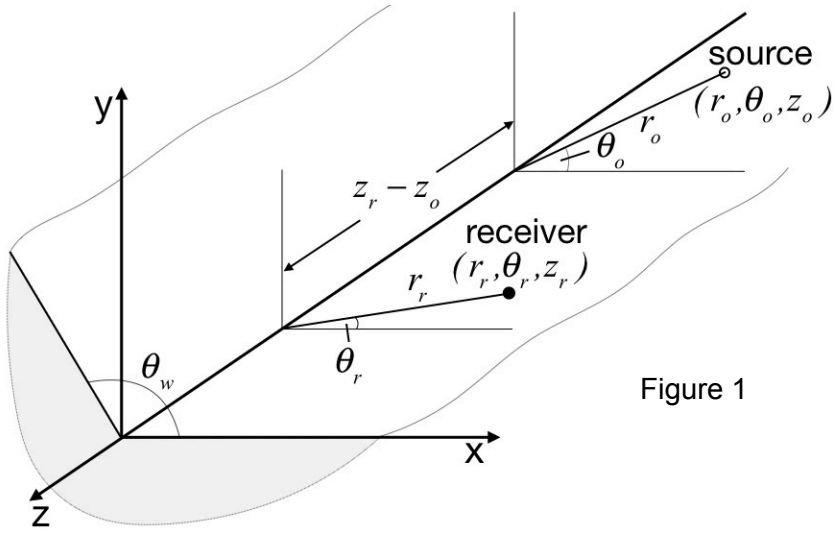

Figure 1

The impulse response solution falls into three time regions. When $t < t_0$, no field is detected. When $t_0 \le t \le \tau_0$, a direct arrival and reflected arrivals may occur. These are delta function impulses arriving directly from the source, or from images of the source reflected in the wedge faces with amplitudes modified by the appropriate reflection coefficient. They are computable using geometrical ray methods. When $t \ge \tau_0$, a diffracted field typically occurs, which always arrives *after* any direct/reflected arrivals, except when the source-receiver path exactly intercepts the wedge apex so that the two signals arrive simultaneously. However, any small finite deviation in receiver angle would introduce a time delay between the arrivals. The diffracted signal is generated at the wedge apex at the exact moment the incident field reaches it, in order to satisfy the boundary condition at the wedge surfaces.

2.2. Summation expressions for direct/reflected and diffracted arrivals

When $t_0 \le t \le \tau_0$, each term in the summations of Eqns. (1) and (2) can be written as the sum of cosine functions, thereby constituting four delta function Fourier series[3], i.e.,

$$p_{rig/p\text{-}r}(r_r, \theta_r, z_r, t) = \frac{S\rho c}{4\pi r_o r_r \sin\xi} \times \sum_m [R\delta(\xi + \theta_o + \theta_r - 2m\theta_w) + R\delta(\xi - \theta_o - \theta_r - 2m\theta_w) + \delta(\xi + \theta_o - \theta_r - 2m\theta_w) + \delta(\xi - \theta_o + \theta_r - 2m\theta_w)] \ (m = 0, \pm 1, \pm 2, \ldots), \quad (5)$$

where $R = \pm 1$. Equation (5) describes delta function arrivals at the receiver from the source and a number of images of the source reflected in the wedge faces. The combinations of angles θ_o, θ_r, and $2m\theta_w$, correspond to the angular relationships between the receiver and the source and its (allowed) images, where m is an integer whose upper value is limited by the condition $|\xi| \le \pi$ in Eqn.(4)$_1$, which restricts the propagation paths to the direct path, and those physically realizable by means of reflections from the wedge faces.

When $t \ge \tau_0$, diffraction arrivals from the wedge apex are generally detected. In this case, since $n > 0$, ensuring that $e^{-n\nu\eta} < 1$ in Eqn. (3)$_3$, the summations in Eqns. (1) and (2) converge, and may be conveniently summed and combined to obtain[7]:

$$p_{rig/p\text{-}r}(r_r, \theta_r, z_r, t) = -\frac{S\rho c}{8\pi\theta_w r_o r_r \sinh\eta} \times [RD_\nu(++) + RD_\nu(--) + D_\nu(+-) + D_\nu(-+)] \quad (R = \pm 1) \quad (6)$$

where

$$D_\nu(\pm, \pm) \equiv \frac{\sin\nu(\pi \pm \theta_o \pm \theta_r)}{\cosh\nu\eta - \cos\nu(\pi \pm \theta_o \pm \theta_r)} \ . \quad (7)$$

2.3. Overview of the BT time-domain analysis of Babinet's principle

BT can be used to calculate the aggregate acoustic field due to two complementary wedges. When the wedge angle is increased to $\theta_w = 2\pi$, the wedges become infinitesimally thin half-plane screens. The theory then shows how the different physical characteristics of direct arrivals, and diffraction arrivals, directly bear on Babinet's principle in the acoustic case.

Direct arrivals, according to BT, may be described using a geometrical approach, as schematically shown in Figs. 2(a) and 2(b). A direct transmission is represented by a ray passing from source to receiver. In Fig. 2(a), the ray is not intercepted by the half-plane, and is detected. In Fig. 2(b) the ray is blocked by the complementary half-plane. In terms of BT, in the first case the direct transmission is "allowed", while in the second case it is not. The aggregate field obtained by adding the results of these two cases is clearly the same as if there had been no object interposed between the source and receiver. This happens irrespectively of the particular combination of boundary conditions applied at the two half-planes. The first statement of Babinet's principle, i.e., that the aggregate field from two complementary apertures is the same as if neither aperture were present, is thus seen to apply to the *direct* arrival, and this appears trivially true once it is explained.

Figure 2

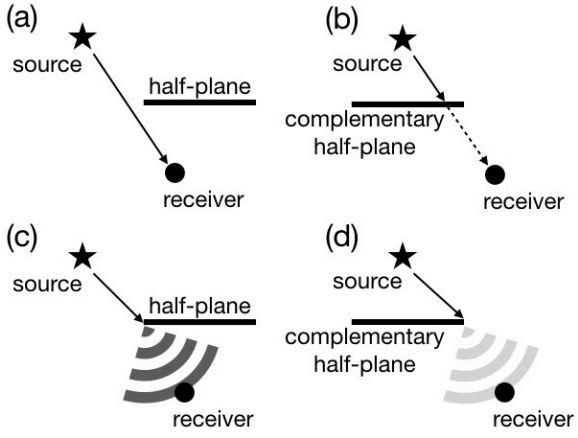

The later diffraction arrivals predicted by BT have a different and more complicated behaviour, shown in Figs. 2(c) and 2(d). For these arrivals, when the diffracted fields of the two half-planes are added, the aggregate field depends on various factors, including the source and receiver angles and the boundary conditions at the half-planes. For the second statement of Babinet's principle to apply, the diffraction amplitudes must exactly cancel to give zero aggregate field. The conditions for this to happen are investigated here.

3. DETAILED ANALYSIS OF BABINET'S PRINCIPLE

3.1. Two horizontally-opposed wedges

Consider two horizontally-opposed infinite exterior wedges, both with external angle $2\pi \geq \theta_w > \pi$, as depicted here. The figures show a slice through the wedges parallel to the $x-y$ plane. The apices of both wedges lie along the z axis and would, if both wedges were present at the same time, meet at the axis passing through the origin O. The right wedge has reflectivity R^R on both upper and lower surfaces, and the left wedge is reversely placed on the negative x-axis, with reflectivity R^L on both surfaces. Figure 3(a) shows the two wedges, and an acoustical source. The source angle is denoted θ_o^R measured counter-clockwise from the upper surface of the right wedge, and θ_o^L measured counter-clockwise from the lower surface of the left wedge. Figure 3(b) shows the same two wedges, with a receiver located below them. The receiver angle is θ_r^R measured counter-clockwise from the upper surface of the right wedge, and θ_r^L measured counter-clockwise from the lower surface of the left wedge. For a source above the wedges, and a receiver below them, simple geometrical arguments show that:

Figure 3

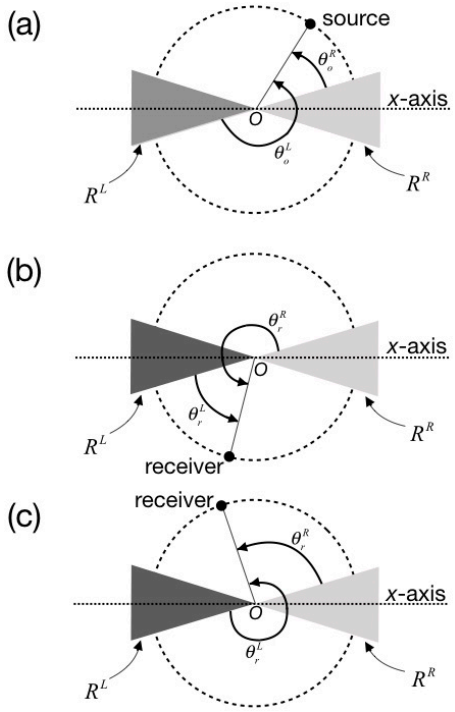

$$\theta_o^L = \theta_o^R + \pi \; ; \; \theta_r^L = \theta_r^R - \pi \quad . \qquad (8)$$

Figure 3(c) shows two wedges with a receiver located above them, so that:

$$\theta_r^L = \theta_r^R + \pi \quad . \qquad (9)$$

3.2. Diffraction from a single half-plane (rigid or pressure-release)

The diffracted field generated by a single rigid, or pressure-release, semi-infinite half-plane on the right-hand side can be computed by letting $\theta_w = 2\pi (\rightarrow \nu = \pi/\theta_w = 1/2)$ in Eqn. (6), and substituting θ_o^R, θ_r^R, to give:

$$p^R(r_r, \theta_r^R, z_r, t) = -\frac{S\rho c}{16\pi^2 r_o r_r \sinh\eta} \times \\ [R^R D_{1/2}(++) + R^R D_{1/2}(--) + D_{1/2}(+-) + D_{1/2}(-+)] \quad , \qquad (10)$$

where $R^R = \pm 1$, and

$$D_{1/2}(\pm\pm) \equiv \frac{\sin\frac{1}{2}(\pi \pm \theta_o^R \pm \theta_r^R)}{\cosh\frac{\eta}{2} - \cos\frac{1}{2}(\pi \pm \theta_o^R \pm \theta_r^R)} \quad . \qquad (11)$$

In the examples shown here, angles are expressed in degrees for the numerical cases considered. In all the examples presented, the parameters $c = r_o = r_r = 1$, $z = 0$, $t = 2.000625$ are used to normalize the calculations for the purposes of illustration and comparison, and to yield $\eta = 0.05$ in Eqn. $(4)_2$ and $\tau_0 = 2$ in Eqn. $(4)_4$. The values $S = 1$ and $\rho = 1$ are also used throughout. Varying the parameters c, r_o, r_r, and z would change the values of η, and thus the field distribution, via Eqn. $(4)_2$ and also Eqn. (10), but not affect the physical argument or conclusions reached.

Figure 4(a) is a polar representation of the angular distribution of the pressure field $p^R(r_r, \theta_r^R, z_r, t)$ diffracted from a semi-infinite half-plane on the right-hand side, with apex lying along the z axis and sides lying in the $x - z$ plane, where $x = 0 \rightarrow +\infty$. The source angle is $\theta_o^R = 49$ deg, and the direction of incidence is indicated. The circular grid line labeled "0" marks zero amplitude, so that both negative (inside this circle) and positive (outside this circle) pressure variations are shown in these plots. The grey curve shows the results for $R^R = +1$, and the dotted curve the results for $R^R = -1$. Consider receiver angle $\theta_r^R = 229$ deg, in the forward scattering direction. For both $R^R = \pm 1$, as θ_r^R increases counter-clockwise through 229 deg, the diffracted pressure amplitudes are first negative, pass through zero, and then become positive. The field forms a diffraction lobe resulting from the shadowing effect of the edge of the half-plane. To emphasize the angle where the shadow region begins, a dashed diametrical line (the "shadow boundary") has been drawn from the source to the opposite side of the plot. A second lobe is seen near $\theta_r^R = 131$ deg. This is associated with acoustic reflections from the side of the half-plane closest to the source. A second diametrical line (the "reflection boundary") has been drawn from the reflected image of the source in the half-plane to the opposite side of the plot. When $R^R = -1$, the amplitude of this lobe changes sign from positive to negative as θ_r^R increases, but, when $R^R = +1$, it changes from negative to positive.

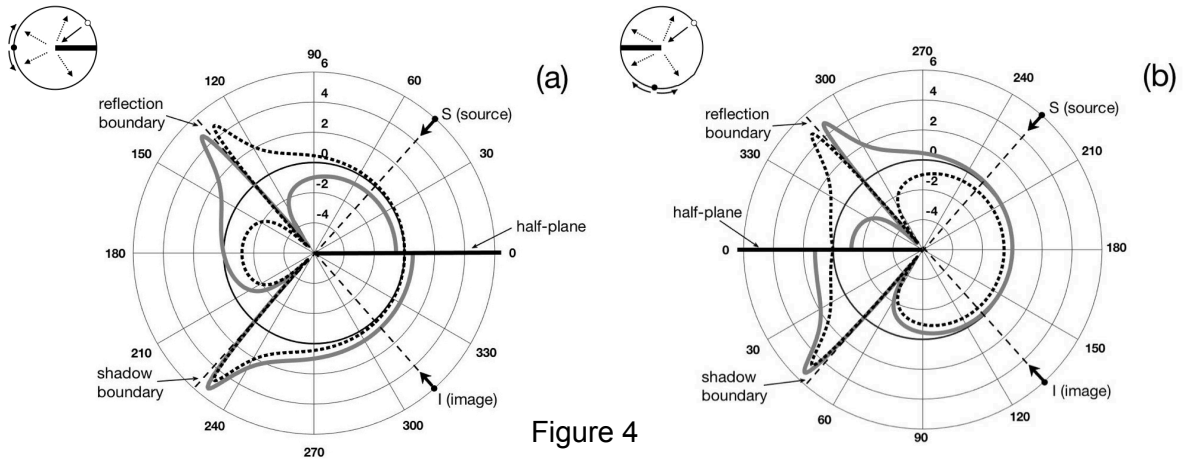

Figure 4

Figure 4(b) shows the corresponding diffracted pressure amplitude $p^L(r_r, \theta_r^L, z_r, t)$ for a reversely placed semi-infinite half-plane on the left-hand side, where $x = 0 \rightarrow -\infty$. The source and receiver angles are now measured counter-clockwise from the lower surface of this half-plane. Here, $\theta_o^L = 229$ deg, and again $R^L = \pm 1$. Two diffraction lobes are again seen, centred on the shadow boundary and reflection boundary. At the shadow boundary ($\theta_r^L = 49$ deg), the amplitude changes from negative to positive as the receiver passes into the geometric shadow (note this now requires a *decrease* in θ_r^L), as was previously observed in Fig. 4(a). At the reflection boundary ($\theta_r^L = 311$ deg), for $R^L = -1$ the sign changes from positive to negative as θ_r^L is decreased clockwise to cross the shadow boundary, while for $R^L = 1$ the sign changes from negative to positive. Both of these cases again correspond with the behaviour seen in Fig. 4(a).

3.3. Aggregated diffraction from two half-planes with opposite reflectivity

For two horizontally-opposed semi-infinite half-planes, Eqns. (8) and (11) yield[8] :

$$\begin{aligned} D^L_{1/2}(++) &= D^R_{1/2}(++) \quad ; \qquad D^L_{1/2}(--) = D^R_{1/2}(--) \ ; \\ D^L_{1/2}(+-) &= -D^R_{1/2}(-+) \quad ; \quad D^L_{1/2}(-+) = -D^R_{1/2}(+-) \, , \end{aligned} \tag{12}$$

where $D^L_{1/2}$, and $D^R_{1/2}$, indicate the evaluation of Eqn. (11) using angles (θ^L_o, θ^L_r), and (θ^R_o, θ^R_r), respectively. For a source of strength S placed in the same location above both half-planes, the aggregate diffracted field detected below the planes is, using the relations in Eqns. (12) to cancel terms:

$$\begin{aligned} p_{AG} &= p^L(r_r, \theta^L_r, z_r, t) + p^R(r_r, \theta^R_r, z_r, t) \\ &= -\frac{S\rho c}{16\pi^2 r_o r_r \sinh\eta} \left(R^R + R^L\right) \left[D^{LR}_{1/2}(++) + D^{LR}_{1/2}(--)\right] \, , \end{aligned} \tag{13}$$

where $D^{LR}_{1/2}$ indicates evaluation of Eqn. (11) using (equivalently) either angles (θ^L_o, θ^L_r) or (θ^R_o, θ^R_r). When $R^R = -R^L = 1$, Eqn. (13) returns $p_T = 0$ identically. Therefore, below the half-plane, the aggregate diffracted field *vanishes* for two half-planes with opposite reflectivity.

For a detector placed above the two half-planes, Eqn. (9) is used in Eqn. (11), and:

$$\begin{aligned} D^L_{1/2}(++) &= -D^R_{1/2}(--) \quad ; \quad D^L_{1/2}(--) = -D^R_{1/2}(++) \, ; \\ D^L_{1/2}(+-) &= D^R_{1/2}(+-) \quad ; \qquad D^L_{1/2}(-+) = D^R_{1/2}(-+) \, , \end{aligned} \tag{14}$$

and the aggregate diffracted field detected above the half-planes is:

$$\begin{aligned} p_{AG} &= p^L(r_r, \theta^L_r, z_r, t) + p^R(r_r, \theta^R_r, z_r, t) \\ &= -\frac{S\rho c}{16\pi^2 r_o r_r \sinh\eta} \times \\ &\quad \left[\left(R^R - R^L\right)\left(D^R_{1/2}(++) + D^R_{1/2}(--)\right) + 2\left(D^{LR}_{1/2}(+-) + D^{LR}_{1/2}(-+)\right)\right]. \end{aligned} \tag{15}$$

When $R^R = -R^L = 1$, Eqn. (15}) indicates that $p_{AG} = 2p^R(r_r, \theta^R_r, z_r, t) = 2p^L(r_r, \theta^L_r, z_r, t)$. Above the two half-planes, therefore, the diffracted fields of both half-planes are identical, and the aggregate diffracted field amplitude is twice that of either of them.

Figure 5(a) shows the angular distribution of the individual and aggregate diffracted pressure amplitudes for two horizontally-opposed half-planes, where $R^R = +1$ and $R^L = -1$. For simplicity, the angles shown are those corresponding to the right-hand half-plane, while the angles for the left-hand half-plane are suppressed. The diffracted fields for both planes are plotted individually, for $\theta^R_o = 49$ deg ($\theta^L_o = 229$ deg), as in Figs. 4(a) and 4(b) (where again the grey curve shows the results for $R^R = +1$, and the dotted curve the results for $R^R = -1$), together with the result of directly adding the two fields together (the black curve). According to Eqn. (13), the aggregate diffraction field below the half-planes should be zero, and this is seen in Fig. 5a. Since the two half-planes cast shadows on opposite sides of the shadow boundary, and there is always a negative to positive change in amplitude of the associated diffraction lobes as the receiver passes into the geometric shadow, and these angular variations also *do not* change sign with the reflectivity, the diffraction lobe amplitudes for the two half-planes vary in opposition to each other in such a way that their sum is exactly zero for all θ^R_r (or θ^L_r) below the half-planes. The reverse behaviour is seen above the half-planes. Equation (15) indicates that the diffraction fields for the two half-planes should vary in an identical manner and reinforce each other when added together. This again is seen in Fig. 5a. Therefore, with respect to the diffraction amplitude, Babinet's principle is seen to apply in the forward scattering direction, but *not* in the back scattering direction.

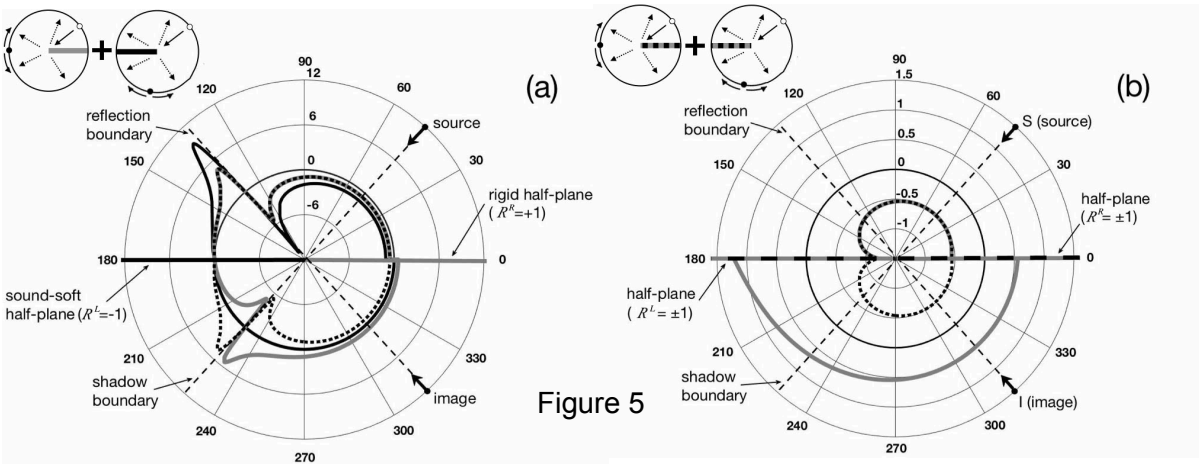

Figure 5

3.4. Aggregated diffraction from two half-planes with the same reflectivity

For two rigid half-planes ($R^R = R^L = 1$), or two pressure-release half-planes ($R^R = R^L = -1$), where a source of strength S is placed above both of them, substitution in Eqn. (13) shows that $p_{AG} \neq 0$ below the half-planes, so that the diffraction field amplitudes no longer cancel, i.e.,

$$p_{AG} = -\frac{S\rho c}{16\pi^2 r_o r_r \sinh\eta}\, 2R^R \left[D^{LR}_{1/2}(++) + D^{LR}_{1/2}(--)\right], \qquad (16)$$

where $R^R = R^L = \pm 1$. The aggregate diffracted field does not now vanish, and the sign of p_{AG} changes with $R^R\ (= R^L)$.

Above the half-planes, Eqn. (15) yields:

$$p_{AG} = -\frac{S\rho c}{8\pi^2 r_o r_r \sinh\eta}\left[D^{LR}_{1/2}(+-) + D^{LR}_{1/2}(-+)\right]\ , \qquad (17)$$

which is again, in general, non-zero. Note that R^R and R^L do not appear in Eqn. (17), so p_{AG} is independent of the reflectivity in this case.

Figure 5(b) shows the angular distribution of the aggregate diffracted pressure amplitudes for two horizontally opposed half-planes of the same reflectivity. The grey curves show the results for: $R^R = R^L = +1$, and the dotted curves show the results for: $R^R = R^L = -1$. The angles are those corresponding to the right-hand half-plane, and $\theta^R_o = 49$ deg ($\theta^L_o = 229$ deg). The diffractions from the individual half-planes are not shown here. While the shadow and reflection boundaries are still indicated, the addition of the individual fields causes the large amplitude variations near these boundaries in the previous figures to partially cancel, resulting in smoothly varying, but non-zero, aggregate fields. Above the half-planes, the curves showing the angular variations for $R^R(= R^L) = \pm 1$ are identical, as indicated by Eqn. (17), while below the half-planes the curves are identical in amplitude, but of opposite sign, in agreement with Eqn. (16).

While, for two complementary half-planes of the same reflectivity, the individual diffraction field amplitudes do not exactly cancel, Babinet's principle may be shown to still apply approximately. Figure 6 shows the individual and aggregate diffraction field amplitudes, below the half-planes, for different combinations of the cases previously shown in Figs. 4(a) and 4(b). In Fig. 6 the curves from Figs. 4(a) and 4(b) are replotted as standard line graphs, together with the results of aggregating them together. The curves labelled with two parameters indicate the aggregate field amplitudes for different combinations of boundary conditions. When $R^R = +1$ and $R^L = -1$, the aggregate field is exactly zero, as expected. If $R^R = R^L = +1$ or $R^R = R^L = -1$, the aggregate field is not zero, but is seen to be typically smoothly-varying and relatively small compared to the variations of the individual diffraction amplitudes near the shadow boundary.

Figure 6

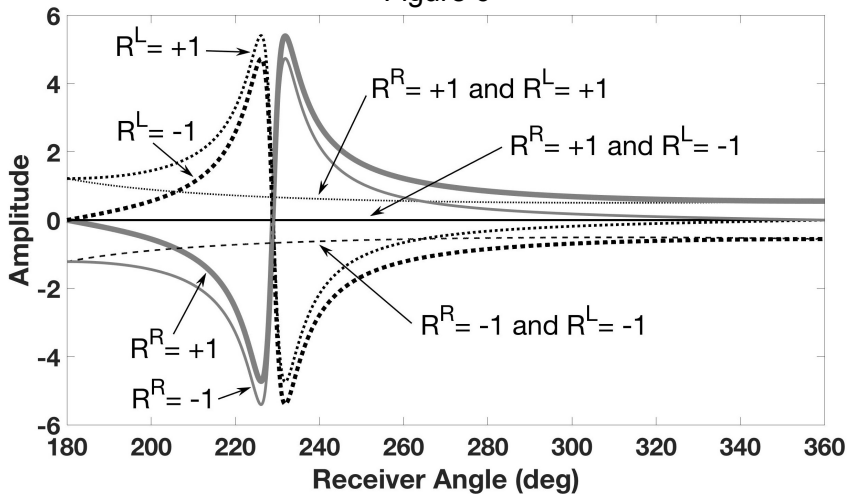

This latter result may facilitate experimental applications of Babinet's principle in acoustics. While it is possible physically to construct thin screens whose surfaces can be treated as practically rigid, it would appear to be very difficult to produce a corresponding screen with upper and lower pressure-release surfaces. However, this result shows that Babinet's principle may be applicable *approximately* if two complementary rigid screens are used.

3.5. Variations of the diffraction intensity

For a receiver placed below two half-planes of opposite reflectivity, Eqn. (13) shows that $p_{AG} = p^L(r_r, \theta_r^L, z_r, t) + p^R(r_r, \theta_r^R, z_r, t) = 0 \Longrightarrow p^L(r_r, \theta_r^L, z_r, t) = -\,p^R(r_r, \theta_r^R, z_r, t)$, and since the sound intensity $I \propto p^2$, the angular distribution of diffraction intensity due to the two planes is identical. Above the half-planes, Eqn. (15) shows that $p^L(r_r, \theta_r^L, z_r, t) = p^R(r_r, \theta_r^R, z_r, t)$, and again the intensity distribution is the same. Therefore, with respect to diffraction intensity, when $R^R = -\,R^L = \pm\,1$, Babinet's principle applies both in the forward *and* back scattering directions.

Below two half-planes with the same reflectivity, application of Eqns. (10) and (12) shows that $\left[p^L(r_r, \theta_r^L, z_r, t)\right]^2 \neq \left[(p^R(r_r, \theta_r^R, z_r, t)\right]^2$, and the intensity distribution of the two half-planes is not identical. This is also the case for a receiver placed above the two half-planes.

3.6. Physical mechanism underlying Babinet's principle in acoustics

In the Biot and Tolstoy[3] and Kinney *et al*.[6] theories, the angular variations of the diffracted field are described using sinusoidal functions, i.e., either $\cos n\nu\theta_o \cos n\nu\theta_r$, or $\sin n\nu\theta_o \sin n\nu\theta_r$, in Eqns. (1), or (2), respectively. Consider two complementary half-planes as shown in Fig. 5(a), where $\theta_w = 2\pi$ ($\rightarrow n\nu = n\pi/\theta_w = n/2$)), and $t \geq \tau_0$.

For the rigid half-plane on the right-hand side, Eqn. (1), together with Eqn. $(3)_3$, yields:

$$p_{rig}(r_r, \theta_r^R, z_r, t) = -\,\frac{S\rho c}{\pi\theta_w r_o r_r \sinh\eta} \sum_{n=1}^{\infty} \cos\frac{n\theta_o^R}{2} \cos\frac{n\theta_r^R}{2} \sin\frac{n\pi}{2} e^{-\frac{n\eta}{2}} \;; \qquad (18)$$

and for the pressure-release half-plane on the left-hand side, Eqn. (2), together with Eqn. $(3)_3$, yields:

$$p_{p\text{-}r}(r_r, \theta_r^L, z_r, t) = -\,\frac{S\rho c}{\pi\theta_w r_o r_r \sinh\eta} \sum_{n=1}^{\infty} \sin\frac{n\theta_o^L}{2} \sin\frac{n\theta_r^L}{2} \sin\frac{n\pi}{2} e^{-\frac{n\eta}{2}} \quad . \qquad (19)$$

Due to the the $\sin(n\pi/2)$ factor in Eqns. (18) and (19), only odd values of n appear in these summations, which are seen to differ only in the sine and cosine factors. For the forward scattering case, substitution of $\theta_o^L = \theta_o^R + \pi$ and $\theta_r^L = \theta_r^R - \pi$ from Eqn. (8) in Eqn. (19) gives:

$$p_{p\text{-}r}(r_r, \theta_r^L, z_r, t) = -\frac{S\rho c}{\pi\theta_w r_o r_r \sinh\eta} \times (-1) \times \sum_{n=1}^{\infty} \cos\frac{n\theta_o^R}{2} \cos\frac{n\theta_r^R}{2} \sin\frac{n\pi}{2} e^{-\frac{n\eta}{2}} \; ; \qquad (20)$$

and adding Eqns. (18) and (20) immediately shows that $p_{rig}(r_r, \theta_r^R, z_r, t) + p_{p\text{-}r}(r_r, \theta_r^L, z_r, t) = 0$ identically. This cancellation occurs for every term in the summations, and leads also to the cancellation seen for the summed expression, i.e., Eqn. (13), when $R^R = -R^L = 1$.

The values of n appearing in the modal expansion for the two types of half-planes are identical. However, as shown, the rigid boundary condition leads to a cosine expansion, and the pressure-release boundary condition leads to a sine expansion. When an acoustic source is placed in the same location with respect to the edges of both half-planes (as in the cases discussed here), for every value of n that appears, the corresponding partial waves that physically generate the diffraction fields below the two types of half-plane have equal amplitudes but different phases, and identically cancel each other when added together.

4. REFERENCES

1. G. Brooker. Modern Classical Optics, Oxford University Press. (2003).
2. B.B. Baker and E.T. Copson. The Mathematical Theory of Huygens' Principle, American Mathematical Society. (2003).
3. M.A. Biot and I. Tolstoy., 'Formulation of wave propagation in infinite media by normal coordinates with an application to diffraction', J.Acoust.Soc.Am. 29(3) 381-391. (1957).
4. I. Tolstoy and C.S. Clay. Ocean Acoustics, Mc-Graw Hill. (1966).
5. I. Tolstoy. Wave Propagation, Mc-Graw Hill. (1973).
6. W.A. Kinney, C.S. Clay and G.A. Sandness., 'Scattering from a corrugated surface: Comparison between experiment, Helmholtz-Kirchhoff theory, and the facet-ensemble method', J.Acoust.Soc.Am. 73(1) 183-194. (1983).
7. H. Medwin and C.S. Clay. Acoustical Oceanography, Academic Press. (1997), pp. 528-532.
8. J. Wielandt. "Time Domain Investigations of Babinet's Principle in Acoustics", Baccalaureate Practical Report. Pontificia Universidad Católica de Chile (2017).